Supplementary Materials for "Pressure-induced band-gap evolution governed by competing orbital coupling and lattice anharmonicity in Cu/Ag-stuffed zinc-blende X_2YZ compounds"

Fang Lyu[1], Xiaolu Zhu[2], Fangqi Liu[1], Tan Peng[2], Yue Hou[2], LingMiao[3], Wei Cao[1,2*], Ziyu Wang[1,2*] and Rui Xiong[1*]

[1]*Key Laboratory of Artificial Micro- and Nano-structures of Ministry of Education, School of Physics and Technology, Wuhan University, Wuhan 430072, People's Republic of China*

[2]*School of integrated circuits, Wuhan University, Wuhan 430072, People's Republic of China*

[3]*School of Optical and Electronic Information, Huazhong University of Science and Technology, Wuhan 430074, People's Republic of China*

Corresponding author: wei_cao@whu.edu.cn

Corresponding author: zywang@whu.edu.cn

Corresponding author: xiongrui@whu.edu.cn

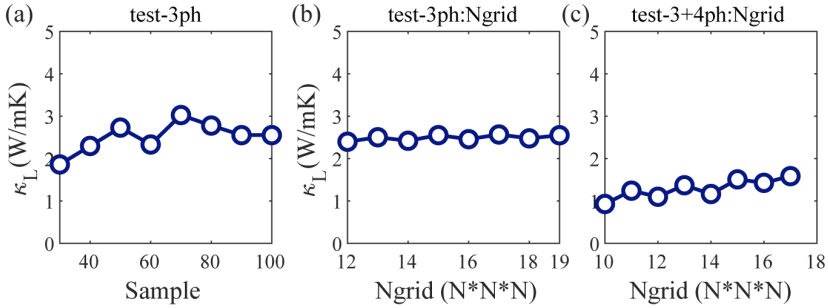

Figure S 1 Test of lattice thermal conductivity κ_L for Li_2CuSb with (a) different samples and Ngrid points for the (b) 3ph and (c) 3+4ph processes at 300 K.

Table S 1 Calculated effective masses (m^*) for *n*-type (electron) and *p*-type (hole) carriers in Li_2CuAs and Li_2CuSb.

	L(a=b)	Carrier type	$\lvert m^* \rvert$
Li_2CuAs	a_0	*n*	0.061
		p	0.162
	a_0-3%a_0	*n*	0.291
		p	0.174
Li_2CuSb	a_0	*n*	0.572
		p	0.143
	a_0-3%a_0	*n*	0.701
		p	0.154

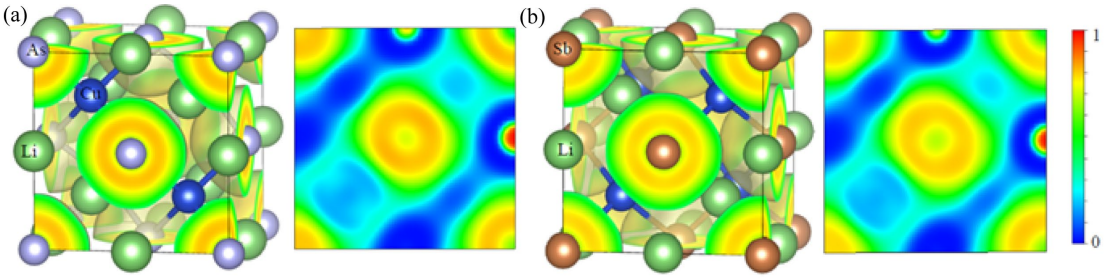

Figure S 2 Calculated projected two-dimensional (2D) electron localization function of (a) Li_2CuAs and (b) Li_2CuSb.

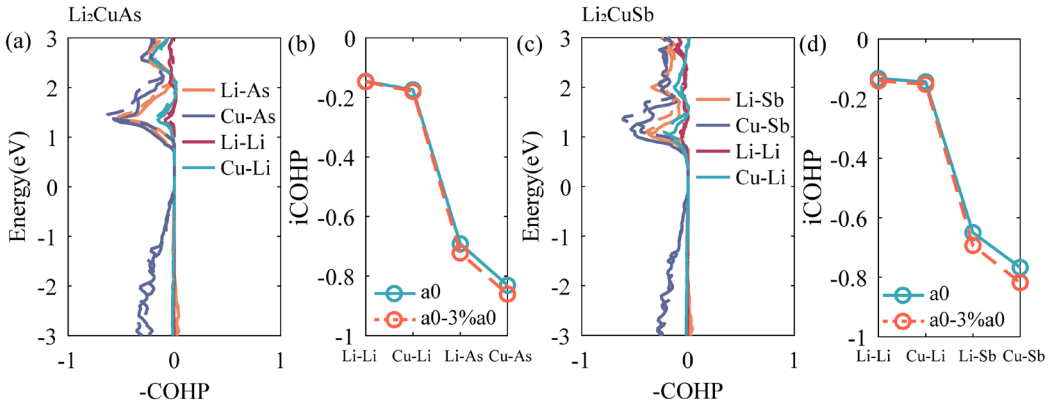

Figure S 3 Crystal orbital Hamilton population (COHP) bonding analysis with integrated crystal orbital Hamilton population (iCOHP) values for (a)-(b) Li_2CuAs, and (c)-(d) Li_2CuSb.

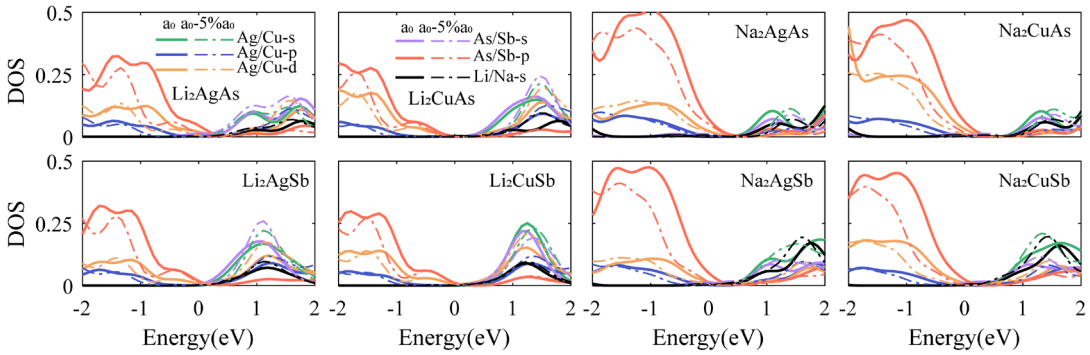

Figure S 4 Projected density of states of X_2YZ compounds with HSE06 hybrid functional.

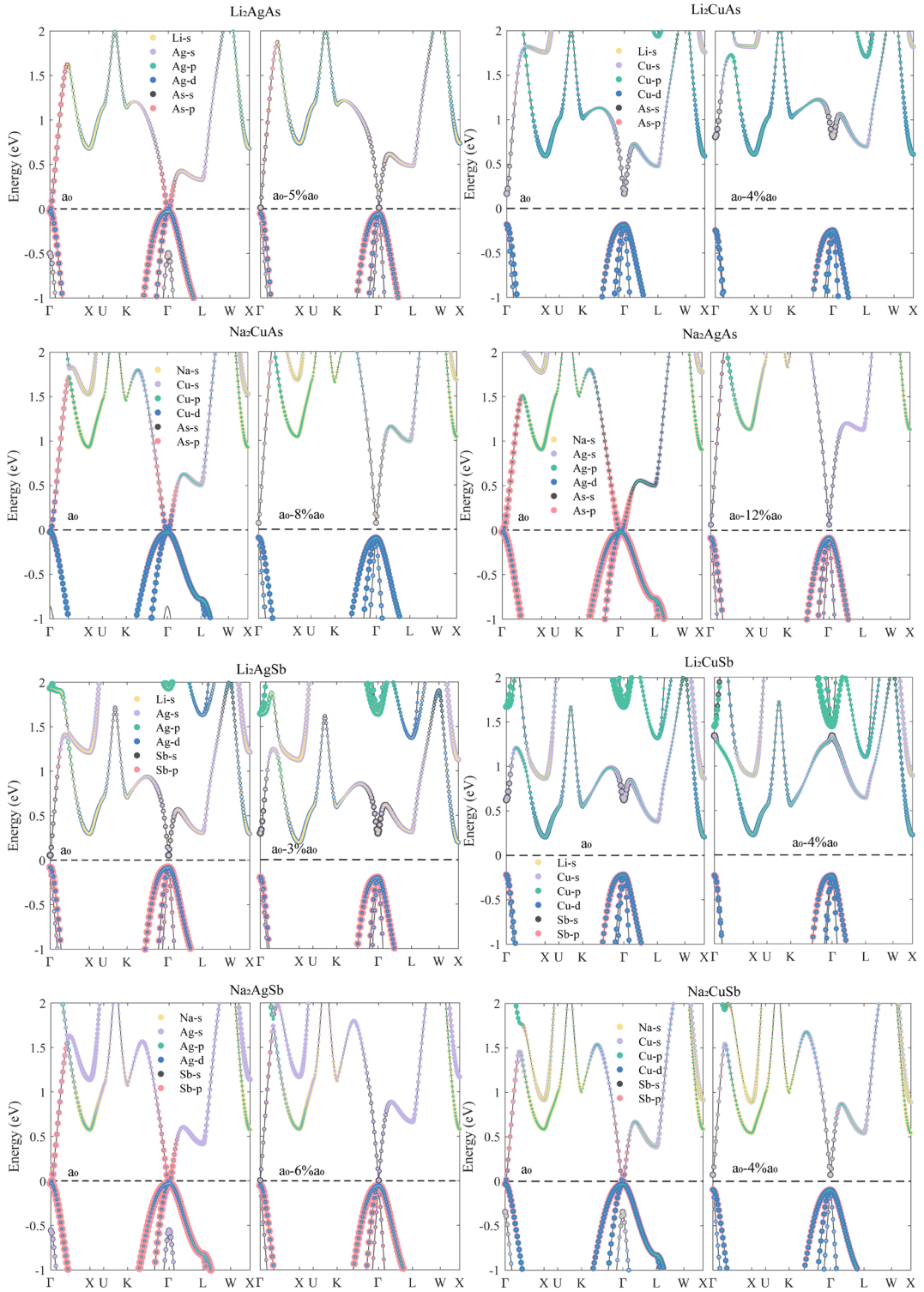

Figure S 5 Orbital-projected band structures of X_2YZ compounds compared between the intrinsic state and that under volume contraction, calculated with the PBE functional.

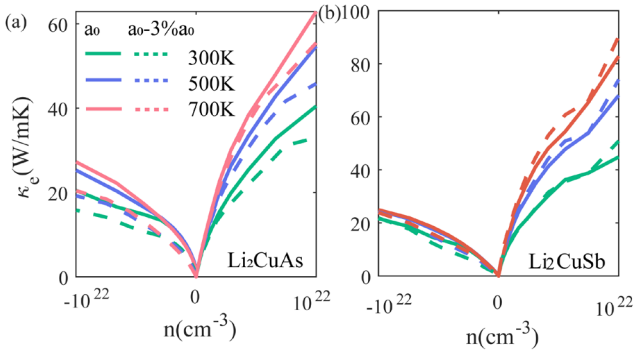

Figure S 6 Electron thermal conductivity (κ_e) as a function of carrier concentration (n) for (a) Li_2CuAs and (b) Li_2CuSb at 300 K, 500 K, and 700 K.

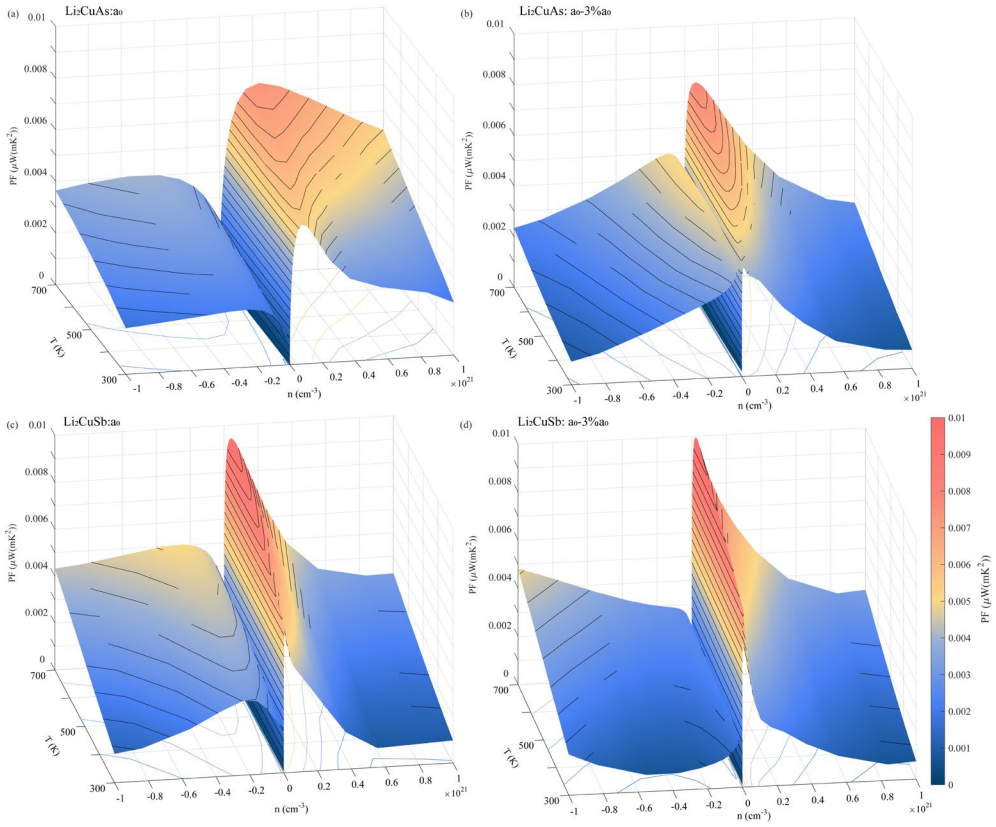

Figure S7 The power factor (PF = $S^2\sigma$) as a function of carrier concentration (n) and temperature (T) for (a)-(b) Li_2CuAs and (c)-(d) Li_2CuSb, comparing the intrinsic state and that under volume contraction.

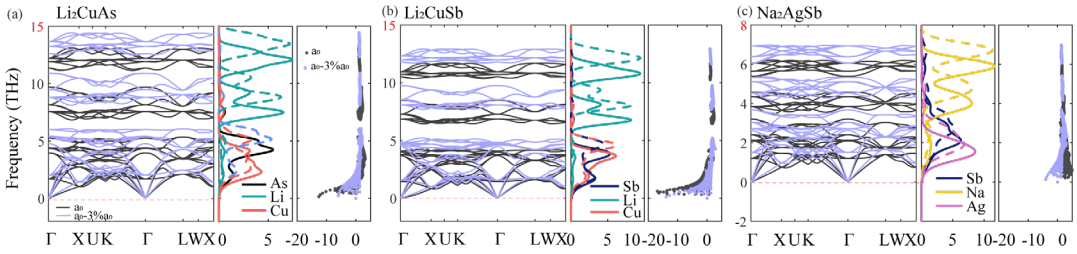

Figure S 8 Phonon dispersions, density of states (DOS), and Grüneisen parameter as a function of frequency for (a) Li_2CuAs, (b) Li_2CuSb, and (c) Na_2AgSb in the intrinsic state and under volume contraction.

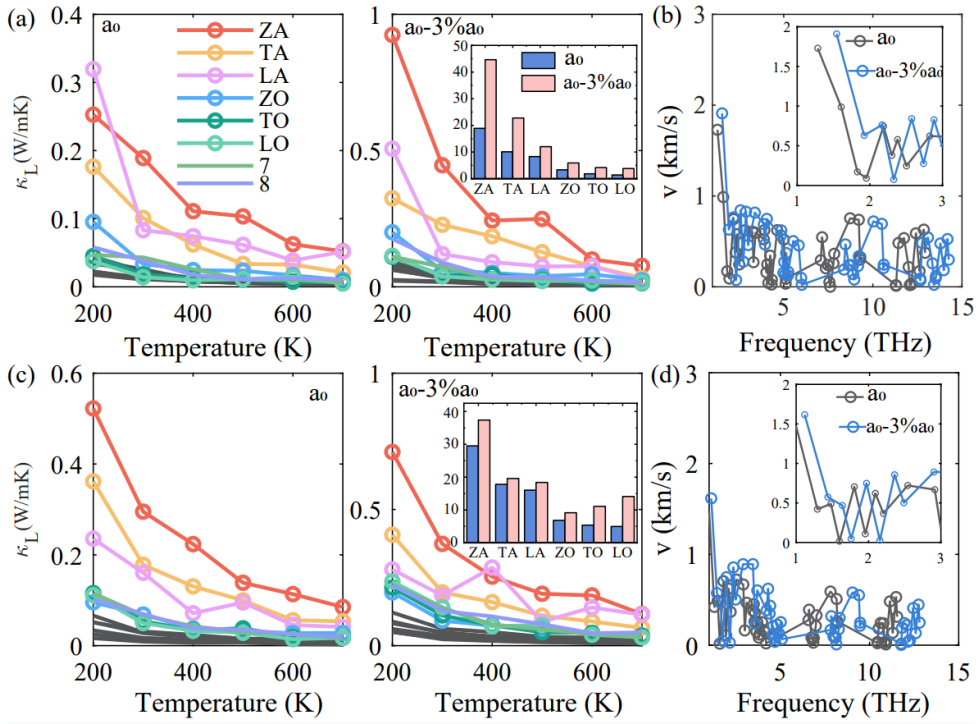

Figure S 9 Temperature-dependent lattice thermal conductivity κ_L in the intrinsic state and under volume contraction, and phonon group velocity. Percentage contributions from different phonon branches in (a)-(b) Li_2CuAs and (c)-(d) Li_2CuSb respectively.

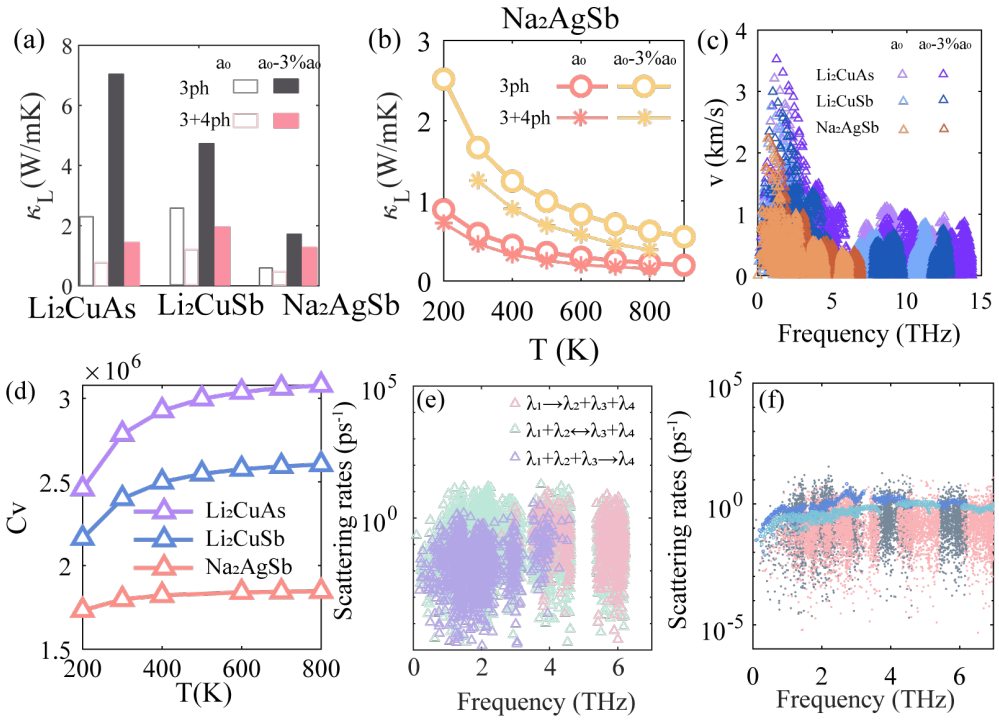

Figure S 10 (a) Comparison of κ_L values calculated using the 3ph and 3+4ph models for Li_2CuAs, Li_2CuSb, and Na_2AgSb. The κ_L versus temperature from ShengBTE simulations. (c) Group velocities as a function of frequency. (d) Phonon heat capacity versus temperature. (e) Anharmonic phonon scattering rates of the intrinsic structures including allowed 3+4ph scattering channels, and (f) anharmonic phonon scattering rates under pressure from the 3ph and 3+4ph models for Na_2AgSb.